



**HAL**  
open science

## Electronic structure and optical properties of isolated and TiO<sub>2</sub>-grafted free base porphyrins for water oxidation

Syrine Daoudi, Abderrahmane Semmeq, Michael Badawi, Xavier Assfeld, Youssef Arfaoui, Mariachiara Pastore

► **To cite this version:**

Syrine Daoudi, Abderrahmane Semmeq, Michael Badawi, Xavier Assfeld, Youssef Arfaoui, et al.. Electronic structure and optical properties of isolated and TiO<sub>2</sub>-grafted free base porphyrins for water oxidation: A challenging test case for DFT and TD-DFT. *Journal of Computational Chemistry*, 2019, 40 (29), pp.2530-2538. 10.1002/jcc.26027 . hal-02395781

**HAL Id: hal-02395781**

**<https://hal.science/hal-02395781>**

Submitted on 12 Nov 2021

**HAL** is a multi-disciplinary open access archive for the deposit and dissemination of scientific research documents, whether they are published or not. The documents may come from teaching and research institutions in France or abroad, or from public or private research centers.

L'archive ouverte pluridisciplinaire **HAL**, est destinée au dépôt et à la diffusion de documents scientifiques de niveau recherche, publiés ou non, émanant des établissements d'enseignement et de recherche français ou étrangers, des laboratoires publics ou privés.

# Electronic structure and optical properties of isolated and TiO<sub>2</sub>-grafted free base porphyrins for water oxidation: a challenging test case for DFT and TD- DFT

**Syrine Daoudi<sup>1,2</sup>, Abderrahmane Semmeq,<sup>1,3</sup> Michael Badawi,<sup>1</sup> Xavier Assfeld<sup>1</sup>, Youssef**

**Arfaoui,<sup>2</sup> Mariachiara Pastore <sup>1</sup>**

Correspondence to: Mariachiara Pastore (E-mail: [mariachiara.pastore@univ-lorraine.fr](mailto:mariachiara.pastore@univ-lorraine.fr))

<sup>1</sup>CNRS & Université de Lorraine, Laboratoire de Physique et Chimie Théoriques (LPCT),

Boulevard des Aiguillettes, BP 70239 54506 Vandoeuvre-lès-Nancy Cedex, France

<sup>2</sup>Laboratory of Physical Chemistry of Condensed Materials, Faculty of Mathematical, Physical  
and Natural Sciences of Tunis, University of Tunis El Manar, Campus Farhat-Hached, 1068

Tunis, Tunisia

<sup>3</sup>Laboratoire Physique de la Matière Condensée, Faculté des Sciences Ben M'sik, Université

Hassan II de Casablanca, Morocco.

## ABSTRACT

Seven free base porphyrins employed in dye-sensitized photoelectrosynthetic cells are investigated with the aim of benchmarking the ability of different Density Functional Theory and Time Dependent Density Functional Theory approaches in reproducing their structure, vertical and  $E_{0.0}$  excitation energies and the energy levels alignment (red-ox properties) at the interface with the  $\text{TiO}_2$ . We find that both vertical and  $E_{0.0}$  excitation energies are accurately reproduced by range-separated functionals, among which the  $\omega\text{B97X-D}$  delivers the lowest absolute deviations from experiments. When the dye/ $\text{TiO}_2$  interface is modeled, the physical interfacial energetics is only obtained when the B3LYP functional is employed; on the other hand, M06-2X (54% of exchange) and the two long-range corrected approaches tested (CAM-B3LYP and  $\omega\text{B97X-D}$ ) excessively destabilize the semiconductor conduction band levels with respect to the dye's lowest unoccupied molecular orbitals (LUMOs), predicting no pathway for electron injection.

## INTRODUCTION

Harvesting solar energy through photovoltaic (PV) devices is the most reliable answer to the necessity of environmentally compatible energies of the future. Among the PV technologies, the possibility of directly producing fuels ( $\text{H}_2$ ,  $\text{CH}_4$ ,  $\text{C}_2\text{H}_6$ , etc.) from sunlight, by exploiting photocatalytic reduction of water or  $\text{CO}_2$ , could provide a scalable grid storage technological platform. In this context, dye-sensitized photoelectrosynthetic cells (DS-PECs) represent an attracting possibility of exploiting the flexibility and tunability of molecular assemblies in light

harvesting and catalysis and the high stability and good charge separation properties of solid-state semiconductors.<sup>[1-5]</sup> Figure 1 displays a schematic representation of a tandem DS-PEC, where, similarly to the architecture of a Grätzel solar cell,<sup>[6]</sup> molecular systems (dyes and catalyst) are grafted on the surface of a mesoporous wide band gap metal oxide (usually TiO<sub>2</sub> and NiO for the photoanode and photocathode, respectively).<sup>[7-10]</sup> At the photoanode, upon solar light absorption by the dye, the photoexcited electrons are transferred to the TiO<sub>2</sub> conduction band (CB), with the associated holes injection into the water oxidation catalyst (WOC). The injected electrons reach then the photocathode, where, upon dye' s excitation, the electrons are transferred to the hydrogen evolving catalyst (HEC) and the holes to the p-type (NiO) semiconductor valence band (VB).<sup>[11-13]</sup>

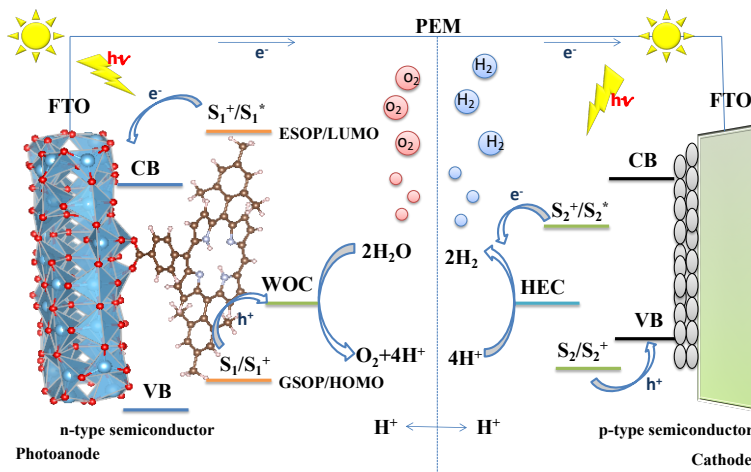


**Figure. 1** Working mechanism of a DSPEC; S indicates the photosensitizer, WOC is the water oxidation catalyst, HEC the hydrogen-evolving catalyst and PEM the proton exchange membrane.

At the base of efficient dye-sensitized photoelectrodes there is the optimal integration of the three main components: the dye sensitizer, the semiconductor and the catalyst.<sup>[14-17]</sup> While the development of molecular components (catalysts and sensitizers) for the proton reduction half reaction has reached important advances over the last years<sup>[18-21]</sup> and the main limiting factor on the photocathode side is represented by the non-optimal characteristics of the p-type semiconductor (NiO),<sup>[13,22-24]</sup> the four-electron water oxidation reaction, requiring the accumulation of four oxidative equivalents at a catalyst site in competition with back electron transfer of injected electrons to the oxidized dye-catalyst assembly,<sup>[4,9,25-28]</sup> is the main bottleneck toward the design of efficient and stable water splitting devices. To assure effective light harvesting and interfacial charge (electron/hole) separation, the dye sensitizer should possess a wide and intense optical absorption spectrum, extending to the red and near infra-red regions, a long-lived charge-separated excited state, possibly strongly electronically coupled to the oxide CB states, and ground and excited state oxidation potentials which properly match the redox potential of the catalyst and the semiconductor CB/VB, Figure. 1. Most of DS-PECs reported so far are based of Ru(II)-polypyridyl complexes,<sup>[29-32]</sup> which are historically the most employed as dye sensitizers in DSSCs, with solar to electric power efficiencies exceeding 11%.<sup>[33]</sup> In view of large scale applications, however, Ru-based dyes present major drawbacks such as low-abundance, high cost and toxicity. The design of efficient metal-free organic dyes is, thus, of primary interest, in virtue of raw materials abundance, generally high synthetic yields and easy tunability of their optical and redox properties. While the utilization of full organic sensitizers has been extensively studied and optimized in conventional DSSCs,<sup>[34-40]</sup> only limited interesting applications have been reported in water oxidation devices.<sup>[26,41]</sup> In this context, promising porphyrin and phthalocyanine derivatives have been reported in combination with different WOCs.<sup>[42-47]</sup> Interestingly, Mallouk

and co-workers reported<sup>[43]</sup> on the use of a series of metal-free porphyrin derivatives (H2Por) as sensitizers on TiO<sub>2</sub> anatase nanoparticles, adopting a co-loaded IrO<sub>2</sub> catalyst. Under visible and red-light irradiation, the majority of the porphyrin-sensitized electrodes produced photocurrents, even if lower than that of the [Ru(bpy)<sub>2</sub>(4,4'-(PO<sub>3</sub>H<sub>2</sub>)<sub>2</sub>bpy)] sensitized photoanode, and large open-circuit voltages (V<sub>oc</sub>). Lower injection yields and lower hole transport within the dye monolayer were regarded as the main reasons limiting the photocurrent generation.<sup>[43]</sup>

Over the last decades, theoretical and computational modelling, essentially based on Density Functional Theory (DFT) and Time-Dependent DFT (TD-DFT), has successfully assisted the experimental research in boosting the DSSCs technology, by providing accurate material's optical and red-ox properties prediction,<sup>[35,48-51]</sup> atomistic insights into the surface sensitization mechanism,<sup>[52-54]</sup> as well as reliable models for the simulation of interfacial injection and recombination processes.<sup>[55-60]</sup> Concerning the spectroscopic properties of the fully organic dyes and the electronic structure of the related dye-sensitized substrates, DFT and TD-DFT methods have been shown to provide a non-coherent description, requiring the use of long-range corrected functionals or hybrids with 40-50% of non-local exchange for the accurate prediction of the optical properties and hybrids with 20-25% of non-local exchange (B3LYP, PBE0, etc...) to deliver a physical and quantitative energy levels lining up at the dye/semiconductor interface.<sup>[24,61]</sup> Due to their generally lower performances in DSSCs,<sup>[58,62,63]</sup> less attention has been paid to free bases porphyrins and to the systematic evaluation of the performances of hybrid functionals in predicting the optical and redox properties of the stand-alone and surface-grafted sensitizers.

Here we consider the seven free base porphyrins (Figure 2) employed in dye-sensitized PECS by Mallouk and co-workers,<sup>[43]</sup> with the aim of benchmarking different TD-DFT approaches in reproducing their structure, vertical and adiabatic excitation energies, as well as the energy levels

alignment (red-ox properties) at the interface with an anatase (101) (TiO<sub>2</sub>)<sub>82</sub> cluster that, as shown in previous works,<sup>[51]</sup> provides a reliable and computationally efficient model for the anatase TiO<sub>2</sub> nanoparticles experimentally employed. The results show that for both the vertical and adiabatic excitation energies, the long-range corrected functionals globally deliver the most accurate description, whereas they completely alter the dye/semiconductor interfacial energetics, and, moreover, they are not able to accurately predict the dye's ground and excited state redox potentials.

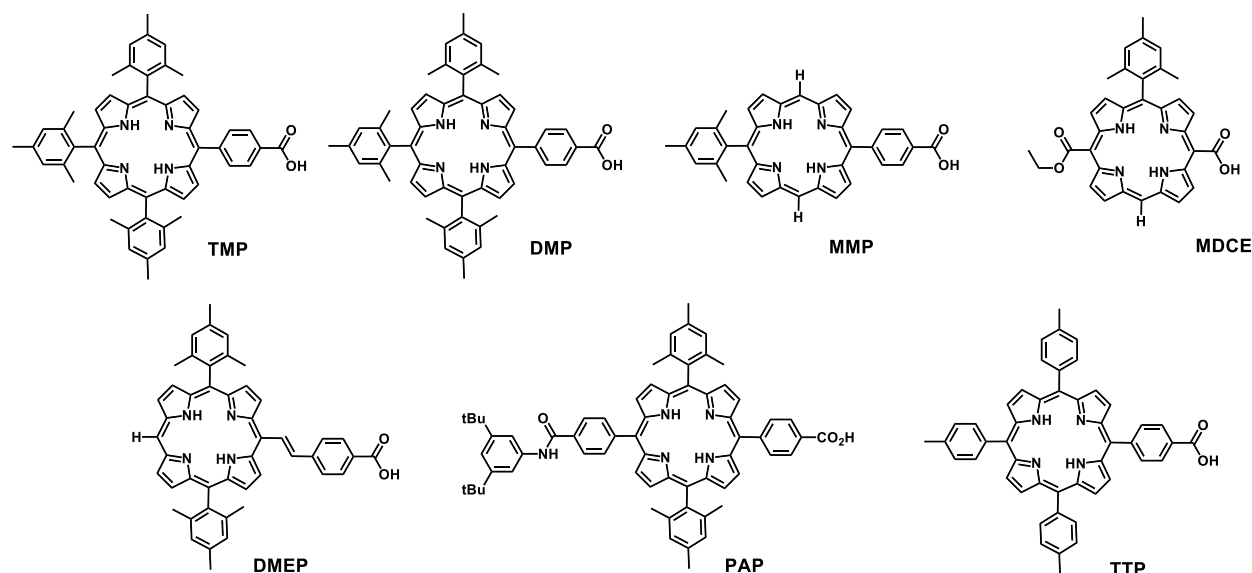


**Figure 2.** Molecular structures and nomenclature of the considered porphyrins.

## COMPUTATIONAL DETAILS

All the calculations on the isolated molecules have been performed with GAUSSIAN 09D software package.<sup>[64]</sup> Adiabatic zero-point vibrational energy (ZPVE) corrected ( $E_{0,0}$ ) and vertical excitation energies (VEE) were calculated by TD-DFT and an implicit description of the solvent (ethyl acetate) according to the C-PCM model<sup>[65]</sup> implemented in Gaussian09. For the ground and

excited state calculations the 6-31G\* basis set was employed, after having confirmed that using larger basis set with diffuse functions 6-31+G\* and the triple zeta quality basis set 6-311G\* both lead to negligible variations<sup>[66]</sup> at the B3LYP<sup>[67]</sup> level of theory on the entire set of molecules (see Table S1 in Supporting Information). The vertical excitation energies of the Q band have been benchmarked using different functionals belonging to various density functional theory classes. Hybrid GGA and meta-GGA functionals such as the B3LYP,<sup>[67]</sup> PBE0,<sup>[68]</sup> HSE06,<sup>[69,70]</sup> BMK,<sup>[71]</sup> TPSSH,<sup>[72]</sup> M06-2X<sup>[73]</sup> and MPW1K<sup>[74]</sup> having a fixed fraction of HF exact exchange; long-range corrected hybrid functionals, namely CAM-B3LYP,<sup>[75]</sup>  $\omega$ B97X-D<sup>[76]</sup> (including Grimme's D2 dispersion correction<sup>[77]</sup>) and LC- $\omega$ PBE.<sup>[78]</sup> Ground state geometry optimizations were carried out at B3LYP/6-31G\* level, this approach being largely assessed to provide accurate ground state structures for both organic and metallorganic compounds.<sup>[61,79,80]</sup> We, however, tested for the largely employed functionals (B3LYP, CAM-B3LYP, M06-2X and MPW1K) the effect of the functional on the ground state equilibrium geometry, by comparing the vertical excitation energies calculated on the resulting optimized structure with those obtained with the same functional on the B3LYP-optimized geometries.  $E_{0,0}$ , were calculated as the energy difference, considering the ZPVE contribution, between the GS and ES at their respective optimized structures in gas phase and ethyl acetate. In this case, five functionals were tested B3LYP,  $\omega$ B97X-D, MPW1K, CAM-B3LYP and M06-2X.

To study the interaction of the molecules with the TiO<sub>2</sub> substrate and evaluate the ability of different DFT methods in providing an accurate estimation of the energy levels alignment at the interface, we optimized the structure of one selected porphyrin, namely DMP, on a TiO<sub>2</sub> slab. The commonly used (TiO<sub>2</sub>)<sub>82</sub> cluster, obtained by appropriately “cutting” an anatase slab exposing the majority (101) surface, was used to model the semiconductor.<sup>[81]</sup> The DMP-(TiO<sub>2</sub>)<sub>82</sub> system was

optimized in gas phase with the ADF program package<sup>[82,83]</sup> employing the PBE exchange-correlation functional<sup>[84]</sup> with a DZP basis set and Grimme's D3 corrections.<sup>[85]</sup> This protocol has been largely shown to deliver reliable dye@semiconductor structures for both inorganic and organic molecular sensitizers.<sup>[59,86,87]</sup> The electronic structure of the DMP-TiO<sub>2</sub> system was modeled by single point calculations on its optimized geometry using two different hybrid functionals, namely B3LYP and M06-2X, and two long-range corrected functionals, CAM-B3LYP and  $\omega$ B97X-D. The 6-311G\* basis was employed for these calculations and the solvent (ethyl acetate) was modeled by employing the C-PCM model,<sup>[65]</sup> as implemented in Gaussian09.<sup>[64]</sup> Estimation of the electron injection times into the TiO<sub>2</sub> have been obtained by using the Newns-Anderson model.<sup>[88]</sup> To apply this model, we need to evaluate the projected density of states (PDOS) relative to the dye's LUMO/LUMO+1 in the dye/TiO<sub>2</sub> complex. The center of this distribution corresponds to the energy of the sensitizer's LUMO/LUMO+1 adsorbed on TiO<sub>2</sub>,  $E_{\text{LUMO}}(\text{ads})$ . On the other hand, the width of the LUMO broadening can be estimated as a mean deviation of a distribution centered at the  $E_{\text{LUMO}}(\text{ads})$  energy value and this gives a direct estimation of the electron-transfer evaluable by using the relation  $\tau(\text{fs}) = 658/\Gamma(\text{meV})$ .

Then, in order to compare the description of the red-ox levels of both the molecule and the substrate obtained by using the single-particle Koopman's approximation, for DMP we also calculated GSOP and ESOP values with the four considered functionals, following the procedure reported in Ref.<sup>[50]</sup>. The ground state oxidation potential (GSOP) for the porphyrins is rigorously computed taking the difference in free energy between the neutral and the oxidized molecules,  $(G^+ - G^0)_{\text{GS}}$ , the free energy in solution ( $G^+$ ,  $G^0$ ) is calculated as  $G = G_{\text{vac}} + \Delta G_{\text{sol}}$  where  $G_{\text{vac}}$  is the Gibbs free energy in vacuo and  $\Delta G_{\text{sol}}$  is the free energy of solvation. The former is obtained by performing a frequency calculation to take into account the vibrational contribution to the total

partition function. The excited state oxidation potential (ESOP) is defined as  $(G^+ - G^0)_{ES}$ , which is the free energy difference between the neutral and oxidized species in their excited state. However, such optimizations become rapidly unavailable due to the huge computational cost, the ESOP could be approximated as  $ESOP = GSOP - E_{0,0}$ , where  $E_{0,0}$  is the ZPVE-corrected adiabatic excitation energy, hence the energy and geometrical reorganization of the excited oxidized species is neglected. The latter procedure could be considered as a vertical approximation to the true ESOP.

## RESULTS AND DISCUSSIONS

### *Isolated porphyrins: vertical Q-band and $E_{0,0}$ excitation energies*

In this section, we discuss the computation of the vertical and ZPVE-corrected adiabatic excitation energies of the seven porphyrin molecules, namely MMP MDCE DMP DMEP TTP TMP and PAP (Figure 2).<sup>143</sup> Porphyrins are highly conjugated macroheterocycles and their electronic absorption spectrum in the 200-800 nm region is characterized by three principal absorption bands.<sup>189,901</sup> The lowest-energy band (500-700 nm), the so-called Q band presents two peaks, labelled, according to their polarization, as  $Q_x$  and  $Q_y$  bands. The most intense absorption corresponds to the Soret Band (or B band), appearing between 370-420 nm and a shoulder on its high-energy tail is instead called N band (330-340 nm). Finally, two weak and broad peaks (L and M bands) appear at higher energies. According to the Gouterman's "four-orbitals model",<sup>191</sup> the low-energy region of the spectrum (Q and B bands) can be described by combination of single excitations from the two highest occupied MOs (HOMO and HOMO-1) to the two lowest unoccupied MOs (LUMO and LUMO+1), depicted in Figure 3 for MMP. The frontier MOs for the other porphyrins are reported in Figure S1 in Supporting information.

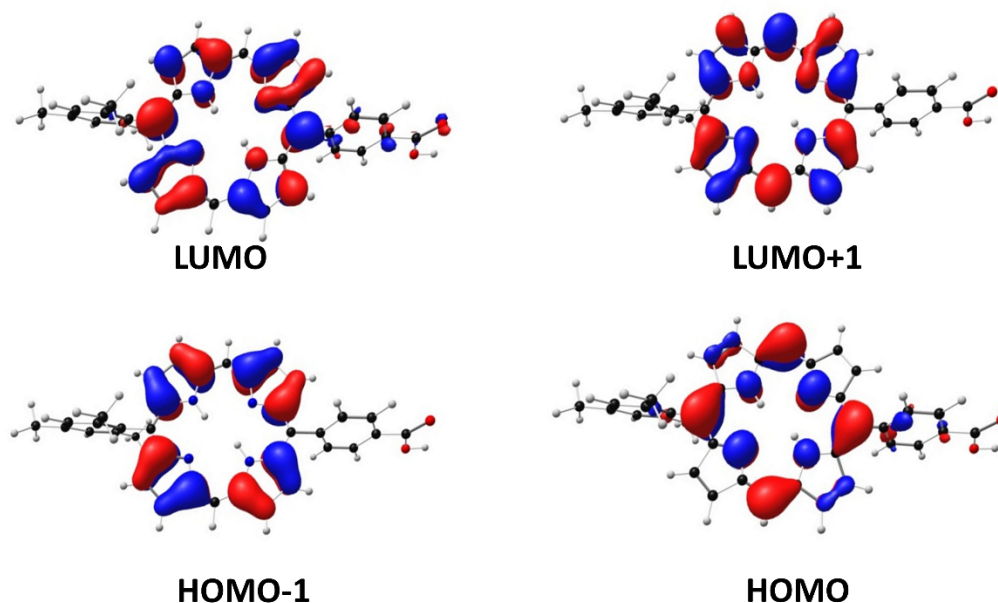


**Figure 3.** Frontier molecular orbitals of **MMP**

Let's start by some remarks concerning the performance of five popular functionals in providing reliable ground state geometries. In Figure 4, the vertical excitation energies calculated by B3LYP, MPW1K, M06-2X and CAM-B3LYP and  $\omega$ B97X-D on top of their respectively optimized ground state structures as well as on top of the B3LYP-optimized ones are compared to the experimental absorption maxima of the  $Q_x$  (top panel) and  $Q_y$  (bottom panel) bands. It is worth to point out here that, the theoretical vertical excitation energy is usually compared with the energy corresponding to the experimental band maximum on the hypothesis of classical vibrations.<sup>[92,93]</sup> This hypothesis is satisfied if the Born-Oppenheimer and Franck-Condon approximations are valid and if the excited state is vibrationally highly excited. Consequently, one should keep in mind that there is always a certain uncertainty when comparing the calculated vertical transition energies with the measured band maxima, while, on the other hand, the calculated  $E_{0-0}$  energies straightforwardly compare with the measured  $E_{0-0}$ . Turning now to the

results, as one could expect due to the strong conjugation and consequent rigidity of the porphyrins core, only small differences are obtained on the vertical excitation energies. Interestingly, the largest differences (0.34 eV) are obtained for the hybrid meta-GGA MPW1K functional, whose equilibrium ground state geometries provide vertical excitation energies less close to the experimental absorption maxima values than those obtained by using B3LYP. Some differences are also obtained with the  $\omega$ B97X-D functional. On the other hand, it is worthwhile to remark that for M06-2X and CAM-B3LYP, being two exchange and correlation functionals peculiarly different from B3LYP, there is an overall excellent agreement between the excitation energies calculated on top of the two geometries. In any case, for all the inspected functionals the B3LYP-optimized geometries globally provided the lowest errors with respect experiments when compared to results obtained using their respective optimized geometries, thus confirming also for these systems the well-known superiority of the B3LYP approach in delivering accurate structural properties.<sup>[80,94]</sup> Thus, the B3LYP-optimized ground state geometries have been employed for the calculation of the vertical excitation energies gathered in Tables 1 and 2 for  $Q_x$  and  $Q_y$ , respectively.

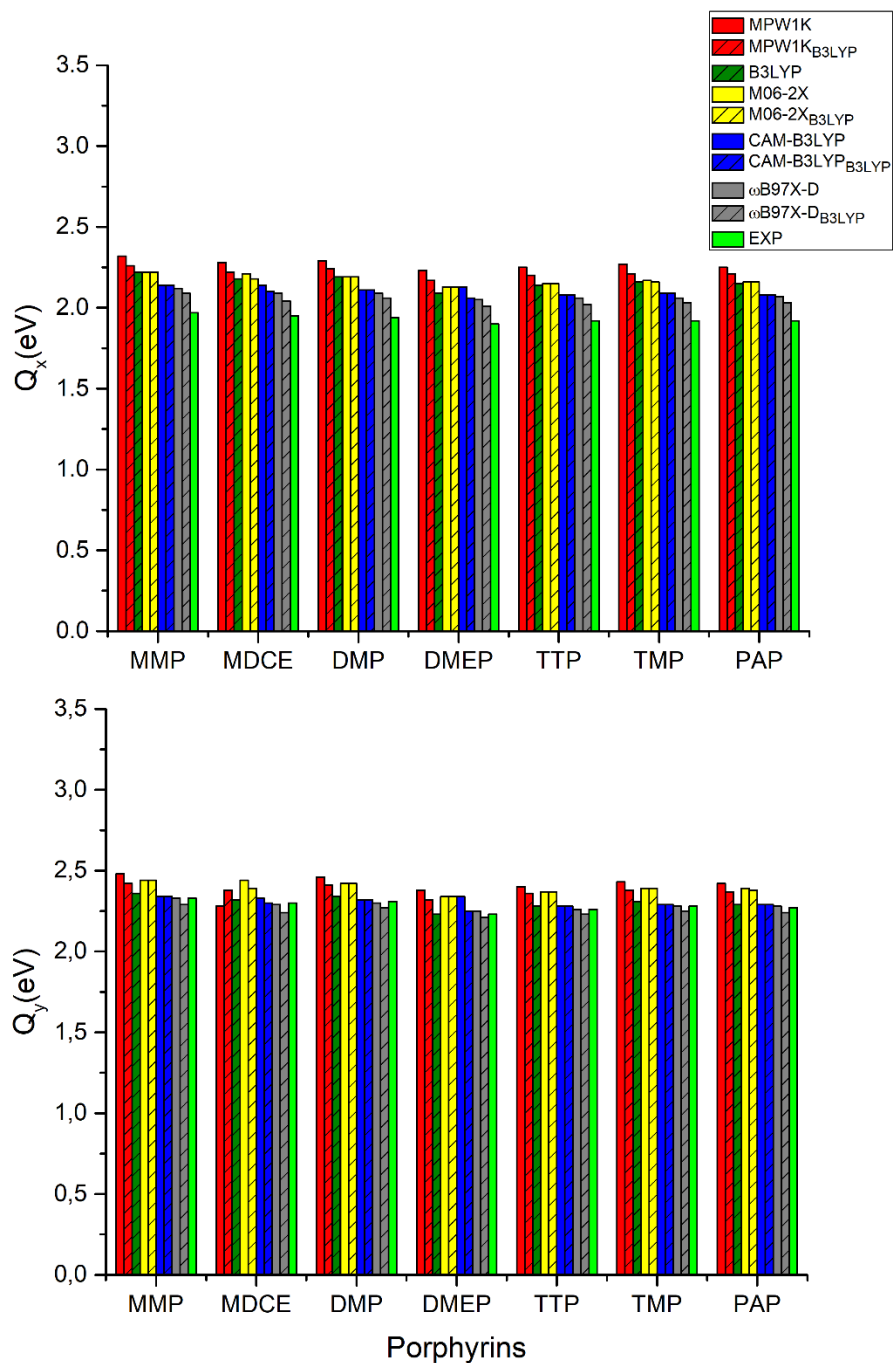


**Figure 4.** Calculated vertical excitation energies for the Q<sub>x</sub> (top) and Q<sub>y</sub> (bottom) bands using different functionals on their respectively optimized ground state geometries (dashed filling) and on the B3LYP optimized geometries (plain filling). The experimental absorption maxima values are also plotted.

As shown by the experimental values, the meso-substitution has only a small effect on the optical properties, like for instance the progressive slight red-shift (0.02-0.03) in the case of MMP, DMP and TMP by addition of each three methyl-phenyl substituent.

**Table 1.** Calculated vertical  $Q_x$  band energies in eV of porphyrins at different levels of theory compared to the experimental band maxima values

	B3LYP	M06-2X	CAM-B3LYP	MPW1K	$\omega$ B97X-D	PBE0	HSE06	BMK	TPSSH	LC- $\omega$ PBE	EXP <sup>a</sup>
<b>MMP</b>	2.22	2.22	2.14	2.26	2.09	2.26	2.26	2.28	2.21	1.84	1.97
<b>MDCE</b>	2.18	2.18	2.10	2.22	2.04	2.21	2.21	2.23	2.16	1.79	1.95
<b>DMP</b>	2.19	2.19	2.11	2.24	2.06	2.23	2.23	2.25	2.18	1.81	1.94
<b>DMEP</b>	2.09	2.13	2.06	2.17	2.01	2.14	2.13	2.18	2.08	1.78	1.90
<b>TTP</b>	2.14	2.15	2.08	2.20	2.02	2.18	2.18	2.20	2.13	1.79	1.92
<b>TMP</b>	2.16	2.16	2.09	2.21	2.03	2.21	2.20	2.22	2.16	1.79	1.92
<b>PAP</b>	2.15	2.16	2.08	2.21	2.03	2.19	2.19	2.21	2.14	1.79	1.92

<sup>a</sup> Ref. [43]

**Table 2.** Calculated vertical  $Q_y$  band energies in eV of porphyrins at different levels of theory compared to the experimental band maxima values

	B3LYP	M06-2X	CAM-B3LYP	MPW1K	$\omega$ B97X-D	PBE0	HSE06	BMK	TPSSH	LC- $\omega$ PBE	EXP <sup>a</sup>
<b>MMP</b>	2.36	2.44	2.34	2.42	2.29	2.41	2.39	2.46	2.34	2.15	2.33
<b>MDCE</b>	2.32	2.39	2.30	2.38	2.24	2.36	2.35	2.41	2.29	2.09	2.30
<b>DMP</b>	2.34	2.42	2.32	2.41	2.27	2.38	2.38	2.44	2.32	2.13	2.31
<b>DMEP</b>	2.23	2.34	2.25	2.32	2.21	2.28	2.26	2.34	2.19	2.07	2.23
<b>TTP</b>	2.28	2.37	2.28	2.36	2.23	2.32	2.31	2.39	2.25	2.09	2.26

<b>TMP</b>	2.31	2.39	2.29	2.38	2.25	2.36	2.35	2.41	2.29	2.10	2.28
<b>PAP</b>	2.29	2.38	2.29	2.37	2.24	2.34	2.33	2.40	2.28	2.10	2.27

<sup>a</sup> Ref <sup>[43]</sup>

As can be seen from the data in Tables 1 and 2, all functionals slightly overestimate the vertical excitation energies with the exception of LC- $\omega$ PBE, showing a systematic underestimation (0.10-0.2 eV) of both  $Q_x$  and  $Q_y$ , and  $\omega$ B97X-D, which slightly underestimates  $Q_x$  (<0.1 eV).

To promptly evaluate the overall performance of the tested functionals, we present in Figure 5 the mean absolute deviations (MAD) with respect to experimental  $Q_x$  and  $Q_y$  band maxima values, it is interesting to note that for  $Q_x$  values most functionals yielded rather high deviations from experimental values. Globally, the higher mean errors (>0.20 eV) have been obtained for the hybrids GGA and meta-GGA functionals, with the BMK method showing the poorest performance and B3LYP, M06-2X and TPSSh delivering comparable accuracy, although possessing quite different amount of Hartee-Fock exchange (20%, 50% and 10% respectively). On overall the long-range corrected functionals tested provide a better description when compared with hybrid functionals and, in particular,  $\omega$ B97X-D yields the lowest error (0.11 eV) for the  $Q_x$  band. In contrast, lower deviations with respect to experimental  $Q_y$  values are obtained for all the functionals; TPSSh gives the best performance with negligible errors (about 0.01 eV) followed by  $\omega$ B97X-D with mean deviation of 0.04 eV. Thus, the long-range and dispersion corrected  $\omega$ B97X-D method appears to definitely outperform with respect to the other functionals considered here, giving a quite accurate prediction of both  $Q_x$  and  $Q_y$  absorption maxima (within the vertical excitation approximation). Considering the localized nature of the lowest energy excited states and the large extension of the  $\pi$  systems, these findings, together with the results discussed above regarding the accuracy on the ground state structures, suggest

that there is a strong interplay of dispersion and long-range Hartree-Fock exchange effects in both the ground and excited states descriptions.

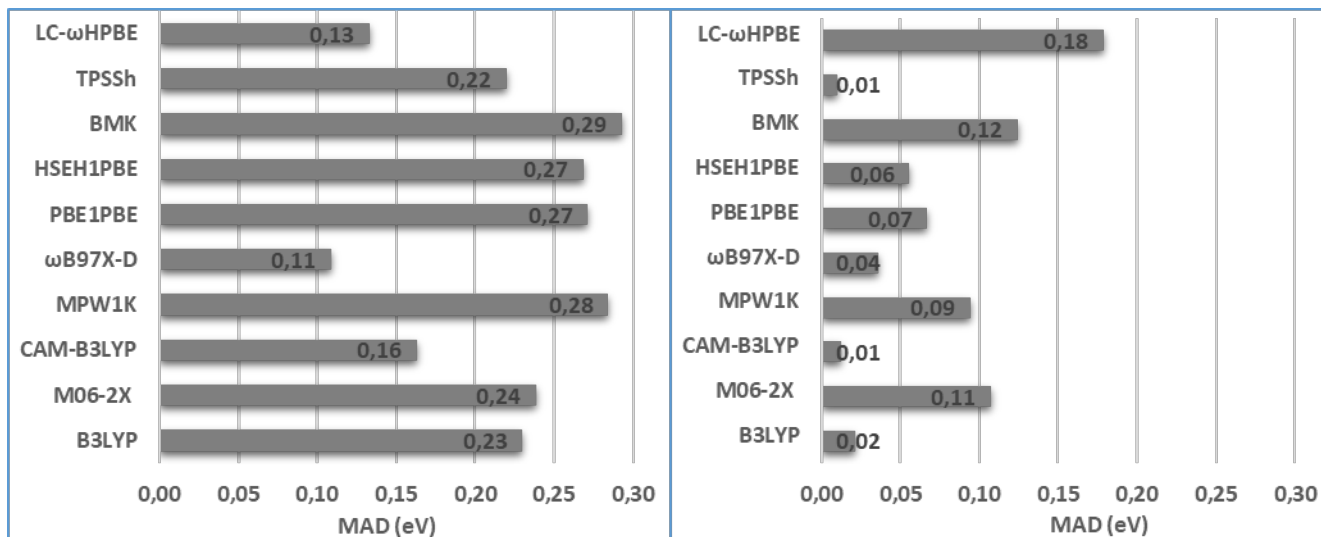


**Figure 5.** Mean absolute deviations (in eV) of the ten functionals tested against experimental  $Q_y$  (left) and  $Q_x$  (right) absorption maxima.

The  $E_{0-0}$  excitation energies computed employing five renowned functionals are listed in Table 3 along with the experimental values.

**Table 3.** Calculated and experimental  $E_{0-0}$  excitation energies in eV.

	B3LYP	CAM-B3LYP	M062X	MPW1K	$\omega$ B97X-D	EXP <sup>a</sup>
<b>MMP</b>	2.12	2.14	2.22	2.27	2.10	1.96
<b>MDCE</b>	2.13	2.08	2.16	2.25	2.06	1.92
<b>DMP</b>	2.17	2.11	2.19	2.24	2.07	1.94
<b>DMEP</b>	2.04	2.06	2.14	2.18	2.03	1.87
<b>TTP</b>	2.10	2.08	2.16	2.20	2.04	1.90
<b>TMP</b>	2.14	2.09	2.16	2.22	2.05	1.91

<b>PAP</b>	2.12	2.08	2.16	2.21	2.04	1.91
------------	------	------	------	------	------	------

<sup>a</sup>: Ref. <sup>[43]</sup>

It can be seen that MPW1K delivered the worst performance with a high mean deviation of 0.31 eV, followed by M06-2X and B3LYP with MAD of 0.26 eV and 0.21 eV respectively (see Figure S2 in Supporting Information). Confirming the trend obtained for the vertical excitations energies, the long-range corrected functionals delivered  $E_{0-0}$  excitation energies closest to the experimental values: CAM-B3LYP yielded a MAD of 0.18 eV and  $\omega$ B97X-D was again confirmed as the most accurate method with a mean deviation of only 0.14 eV with respect to experimental  $E_{0-0}$  energies.

Withstanding these results, the  $\omega$ B97X-D functional, combining long range and dispersion corrections, resulted as the best functional for the computation of optical properties of the investigated porphyrins due to its consistency and balanced performance in the description of both adiabatic and vertical excitation energies, as well as in providing reliable ground and excited state structures. We also note the inferior performances of the hybrids GGA and meta-GGA methods when compared to long-range corrected functionals.

### *DMP-TiO<sub>2</sub>: structure and energy level's lining up*

The optimized ground state structure of DMP adsorbed on the TiO<sub>2</sub> cluster is displayed in Figure 6. This adsorption conformation, with the molecule only slightly bent on the surface, was calculated to be, at B3LYP/6-31G\* level of theory in implicit ethyl acetate, more than 4.5 eV lower in energy with respect to the “flat adsorption” conformation reported as the most stable for other porphyrins.<sup>[95]</sup> This is also in line with the rather high surface coverage of  $0.92 \text{ \AA}^{-2} \sim 10^{-7}$

mol/cm<sup>2</sup> reported in Ref. [43] and comparable to the one of the reference Ru(bpy)<sub>2</sub>(4,4'-(PO<sub>3</sub>H<sub>2</sub>)<sub>2</sub>bpy) dye.

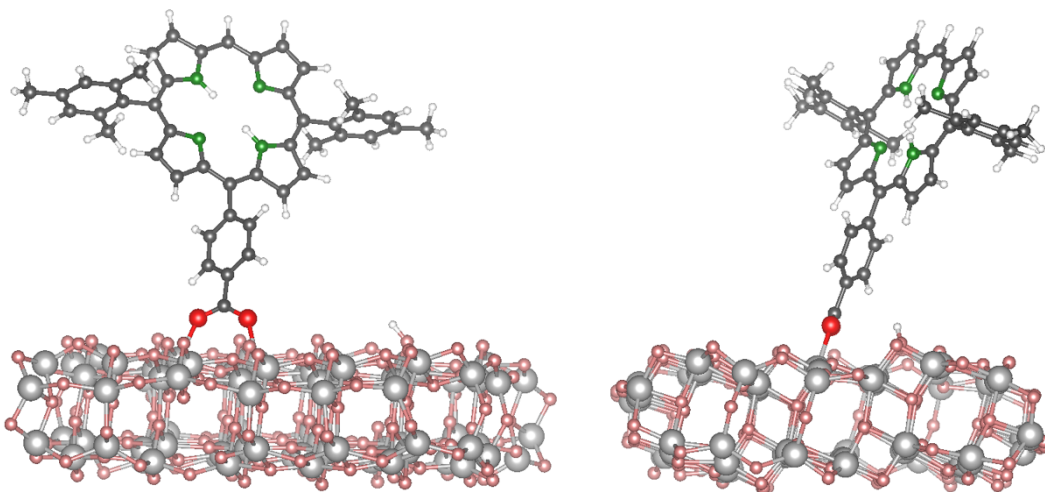


**Figure 6.** Front (left) and side (right) views of the DMP-(TiO<sub>2</sub>)<sub>2</sub> optimized structure. Ti (TiO<sub>2</sub>), O (TiO<sub>2</sub>), C, N, O and H atoms are in light grey, pink, dark grey, green, red and with respectively.

The optimized O-Ti distances are 2.12-2.08 Å, as calculated for other TiO<sub>2</sub>-grafted sensitizers.<sup>[27,39]</sup>

A summary of the relevant energy levels for the isolated and TiO<sub>2</sub>-adsorbed DMP, as well as for the semiconductor is reported in Table 4 against known experimental quantities. For the isolated DMP, we report the HOMO/LUMO and GSOP/ESOP values, while for the DMP-TiO<sub>2</sub> complex we list the HOMO/LUMO values for both the molecule and the semiconductor slab and we also calculated the LUMO\* value, by adding the S<sub>0</sub>→S<sub>1</sub> vertical excitation energy to -ε<sub>HOMO</sub>, to approximate the ESOP. The corresponding calculated projected density of states (PDOS) are displayed in Figure 7.

**Table 4.** Ground state oxidation and reduction potential calculated using the Koopman's theorem ( $-\epsilon_{\text{HOMO}}$ ) and ( $-\epsilon_{\text{LUMO}}$ ), respectively, along with excited state oxidation potential obtained adding the  $S_0 \rightarrow S_1$  vertical excitation energy to ( $-\epsilon_{\text{HOMO}}$ ). All values are in eV. Experimental data (V vs. NHE) are converted in eV against the vacuum by adding 4.44.

<i>Method</i>	<i>DMP-TiO<sub>2</sub></i>		<i>DMP isolated</i>		<i>DMP-TiO<sub>2</sub></i>	
	<b>HOMO</b>	<b>LUMO/LUMO*</b>	<b>HOMO/GSOP</b>	<b>LUMO/ESOP</b>	<b>HOMO</b>	<b>LUMO/LUMO*</b>
<b>B3LYP</b>	5.44	2.67 / 3.25	5.47/5.14	2.72/3.09	7.52	3.25/4.03 <sup>b</sup>
<b>M06-2X</b>	6.44	2.25/4.25	6.47/5.56	2.27/3.25	9.42	2.24
<b>CAM-B3LYP</b>	6.42	1.90/4.31	6.45/5.14	1.92/3.02	9.16	2.02
<b>ωB97X-D</b>	6.92	1.41/4.86	6.95/5.13	1.44/3.14	9.67	1.38
<b>Exp.</b>			<b>5.60<sup>a</sup></b>	<b>3.54<sup>a</sup></b>	<b>7.04</b>	<b>3.84</b>

<sup>a</sup> Ref. <sup>[43]</sup>

<sup>b</sup> Calculated taking the calculated value (B3LYP/3-21G\*/(water) C-PCM) of 3.49 eV for  $S_0 \rightarrow S_1$  from Ref. <sup>[27]</sup>

The picture coming from the data in Table 4 and the energy lining up shown in Figure 7 is rather complicated. Indeed, if one consider the red-ox potentials approximation within the Koopman's scheme, as discussed elsewhere,<sup>[61]</sup> the B3LYP functional, although providing absolute values for both the dye and TiO<sub>2</sub> with deviations of about 0.2-0.5 eV from the experiments, is able to deliver a correct relative alignment between the levels of the dye and those of the substrate. The B3LYP PDOS in Figure 7 show, indeed, the expected interfacial energetics, with the LUMO/LUMO+1 distribution lying at  $\sim -2.7$  eV, well above the conduction band minimum (CBM), calculated at -3.25 eV. The estimated driving force for electron injection (LUMO-CBM) at B3LYP level of theory is 0.52/0.78 eV for the LUMO/LUMO\*, resulting, however, in a slight overestimation with respect to the experimental value of 0.3 eV.

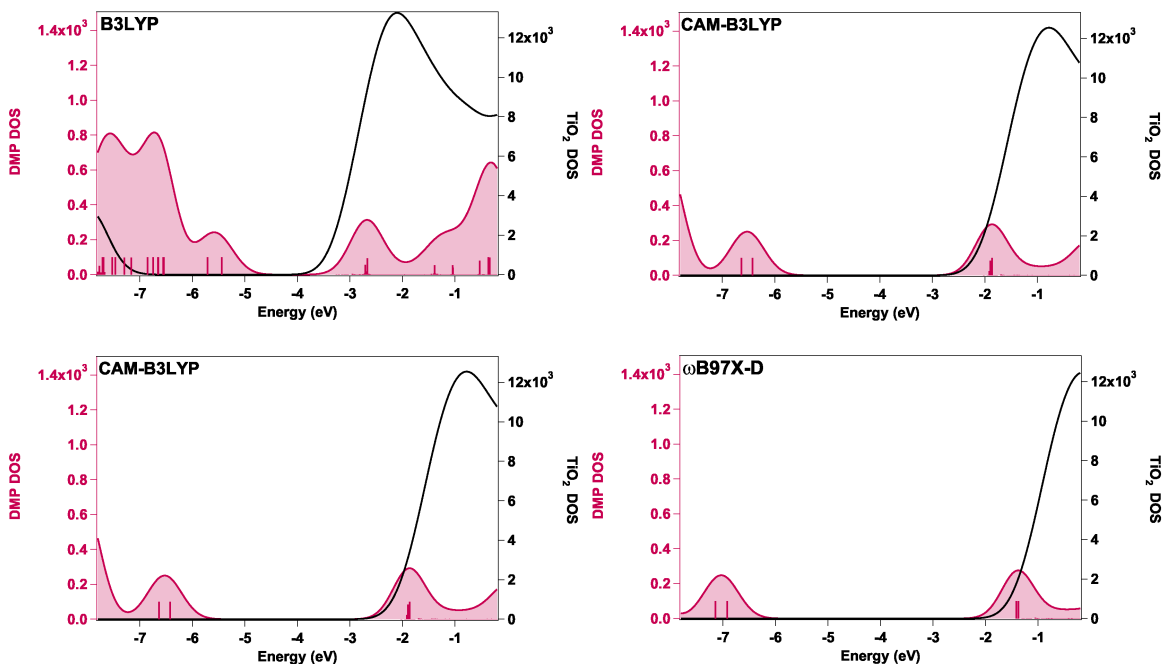


**Figure 7.** Calculated DMP (full red) and TiO<sub>2</sub> (black) partial density of states (PDOS) with the B3LYP, M06-2X, CAM-B3LYP and  $\omega$ B97X-D functionals in ethyl acetate. The PDOS have been convoluted with a gaussian broadening of 0.2 eV.

As is apparent in Figure 8, three strongly hybridized DMP-TiO<sub>2</sub> molecular orbitals are found around -2.70 eV, corresponding to the dye's LUMO, while, for symmetry reasons, an almost pure dye's LUMO+1 level appear at -2.67 eV. Within the Newns-Anderson model, the calculated  $E_{\text{LUMO}}$  for the adsorbed molecule is -2.73 eV, almost coincident with the value calculated for the isolated protonated DMP (Table 4), and the resulting lifetime broadening  $\hbar\Gamma$  is  $4.6 \times 10^{-2}$  eV, with a predicted injection time of about 14 fs. At CAM-B3LYP level of theory, the dye's LUMO is calculated just above the CBM of TiO<sub>2</sub> (-1.90 eV vs 2.02 eV, see Table 4) and thus, lying within the more localized trap states composing the CB edge tail, its mixing with the

semiconductor states is significantly lower, with a lifetime broadening of  $7.1 \times 10^{-3}$  eV and a calculated injection time of about 100 fs.

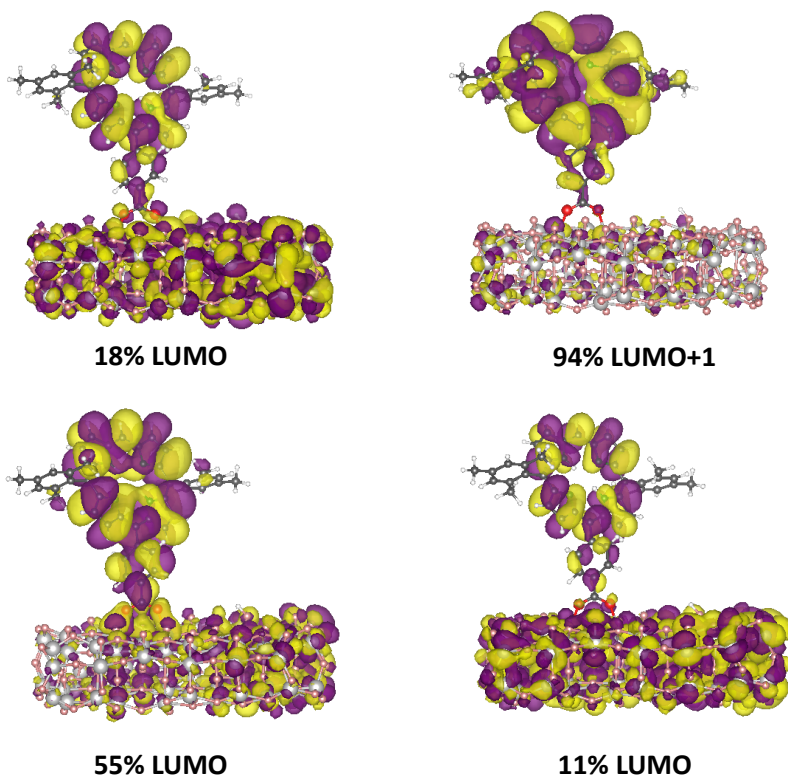


**Figure 8.** Isosurfaces of the DMP-TiO<sub>2</sub> Kohn–Sham B3LYP states mainly localized on the dye and corresponding to the LUMO and LUMO+1 levels.

For both M06-2X and  $\omega$ B97X-D, the LUMO and LUMO+1 are calculated below the TiO<sub>2</sub> CBM, with the former delivering the worse description, as shown by the values in Table 4. This result is interestingly different from the findings discussed for push-pull organic dyes in Ref [96], where at the Kohn-Sham single-particle level the effect of increasing the Hartree-Fock exchange or using a long-range corrected functional (CAM-B3LYP) was producing a rigid up-shift/down-

shift of all the unoccupied/occupied levels (dye and TiO<sub>2</sub>), leaving essentially unaffected both the relative alignment and the electronic coupling. Here the picture is more complicated, with a differential response of the porphyrin and TiO<sub>2</sub> energy levels at the different functionals, translating into a completely altered interfacial energetics as the functional is changed. In this context, although computationally much more expensive, many body perturbation theory, i.e. GW/BSE, calculations have been shown to lead to better agreement with experiments compared to the estimates obtained from the Kohn–Sham eigenvalue.<sup>[97–99]</sup>

Finally, when the rigorously calculated GSOP and ESOP values for the isolated molecule are concerned, M06-2X is the functional providing the better agreement with experiments (see data in Table 4), with deviations of 0.04/0.29 eV for GSOP/ESOP. Surprisingly, B3LYP, CAM-B3LYP and  $\omega$ B97X-D, despite their dramatically different electronic structure description, deliver similar results, significantly underestimating GSOP (~ 0.5 eV) and, consequently, ESOP (0.4-0.5 eV). These large error in computing GSOP and ESOP can be traced back to problems in the accurate calculations of free energy in solution; this is a well-known behavior of DFT functionals with continuum model especially for the oxidized species and solvated excited state computations where errors arising from the level of theory and the solvation model overlap and make it difficult to distinguish both effects. The good performance of M062X in this particular case, most probably, might be due to some error cancellations.

## CONCLUSIONS

We have investigated the structural and optical properties (vertical and E<sub>0-0</sub> excitation energies) of a series of free base porphyrins in solution by employing various exchange and correlation

functionals. We have also evaluated the reliability of two long-range corrected (CAM-B3LYP and  $\omega$ B97X-D) and two hybrid functionals (B3LYP and M06-2X) in delivering a physical energy level's lining up at the molecule/TiO<sub>2</sub> interface for one selected porphyrin. The present results confirm that, in line with previous results, B3LYP is the best choice, among the functionals tested here, to optimize the ground state geometries. When the vertical and E<sub>0-0</sub> excitation energies are considered, long-range corrected approaches provide the closest agreement with experiments, with the  $\omega$ B97X-D functional delivering the lowest MADs. On the other hand, the prediction of the correct relative alignment between the dye's and semiconductor's energy levels, can only be achieved at B3LYP level of theory. Larger fraction of Hartree-Fock exchange (50% in the M06-2X) and long-range corrections, over-destabilize the TiO<sub>2</sub> CB Kohn-Sham levels with respect to the porphyrin's LUMO/LUMO+1 orbitals, completely disrupting the physical interfacial energetics. Then, concerning the calculations of the ground and excited state oxidation potentials of the dye, for the porphyrin considered at the TiO<sub>2</sub> interface, the best agreement with the experimental values was obtained with the M06-2X, while the other three functional tested (B3LYP, CAM-B3LY and  $\omega$ B97X-D) yielded severe underestimations (about 0.5 eV). In this case, we believe that the errors in the calculation of free energies in solution might play a relevant role on the accuracy of the final results. In conclusion, analogously to previous results on push-pull organic sensitizers,<sup>[61]</sup> if one is able on the one hand to reproduce the optical absorption spectra by range-separated functionals, on the other hand the same methodology predicts strongly energetically unfavorable electron injection process for the dye/semiconductor system. By varying the exchange-correlation functional a correct energy offset can be obtained but larger errors on the absorption maximum energy are obtained.

## ASSOCIATED CONTENT

**Supporting information.** Effect of basis set size on the vertical excitation energies employing B3LYP with the double and triple zeta pople basis sets for the porphyrins are reported in Table S1. Values of the computed  $Q_x$  and  $Q_y$  energies along with experimental absorption maxima are presented in tables S2 and S3. In figure S1 we show frontier molecular orbitals of the porphyrin set of molecules, while in figure S2 we present (MAD) with respect to experimental  $E_{0-0}$  excitation energies for five TDDFT functionals. XYZ coordinates of the optimized geometries of all studied porphyrins are gathered in the SI file.

## ACKNOWLEDGMENTS

We thank ANR JCJC HELIOSH2 (ANR-17-CE05-0007-01) for financial support and HPC resources from GENCI-CCRT/CINES (Grants 2018-A0010810139).

## REFERENCES

- [1] J. R. Swierk, T. E. Mallouk, *Chem. Soc. Rev.* **2013**, *42*, 2357–2387.
- [2] M. D. Kärkäs, O. Verho, E. V. Johnston, B. Åkermark, *Chem. Rev.* **2014**, *114*, 11863–12001.
- [3] Y. J. Yuan, Z. T. Yu, D. Q. Chen, Z. G. Zou, *Chem. Soc. Rev.* **2017**, *46*, 603–631.

- [4] P. Xu, N. S. McCool, T. E. Mallouk, *Nano Today* **2017**, *14*, 42–58.
- [5] T. J. Meyer, M. V. Sheridan, B. D. Sherman, *Chem. Soc. Rev.* **2017**, *46*, 6148–6169.
- [6] B. O'Regan, M. Grätzel, *Nature* **1991**, *353*, 737–740.
- [7] F. Li, K. Fan, B. Xu, E. Gabrielsson, Q. Daniel, L. Li, L. Sun, *J. Am. Chem. Soc.* **2015**, *137*, 9153–9159.
- [8] A. Nattestad, A. J. Mozer, M. K. R. Fischer, Y. B. Cheng, A. Mishra, P. Bäuerle, U. Bach, *Nat. Mater.* **2010**, *9*, 31–35.
- [9] Y. K. Eom, L. Nhon, G. Leem, B. D. Sherman, D. Wang, L. Troian-Gautier, S. Kim, J. Kim, T. J. Meyer, J. R. Reynolds, et al., *ACS Energy Lett.* **2018**, *3*, 2114–2119.
- [10] J. T. Kirner, R. G. Finke, *ACS Appl. Mater. Interfaces* **2017**, *9*, 27625–27637.
- [11] M. K. Brennaman, R. J. Dillon, L. Alibabaei, M. K. Gish, C. J. Dares, D. L. Ashford, R. L. House, G. J. Meyer, J. M. Papanikolas, T. J. Meyer, *J. Am. Chem. Soc.* **2016**, *138*, 13085–13102.
- [12] C. S. Ponceca, P. Chábera, J. Uhlig, P. Persson, V. Sundström, *Chem. Rev.* **2017**, *117*, 10940–11024.

- [13] A. M. Brown, L. J. Antila, M. Mirmohades, S. Pullen, S. Ott, L. Hammarström, *J. Am. Chem. Soc.* **2016**, *138*, 8060–8063.
- [14] Z. Yu, F. Li, L. Sun, *Energy Environ. Sci.* **2015**, *8*, 760–775.
- [15] S. Caramori, F. Ronconi, R. Argazzi, S. Carli, R. Boaretto, E. Busatto, C. A. Bignozzi, in *Sol. Energy Convers. Photoelectrochem. Syst.*, Springer, Cham, **2016**, pp. 67–143.
- [16] M. Pastore, *Computation* **2017**, *5*, 5.
- [17] M. Pastore, T. Etienne, F. De Angelis, *J. Mater. Chem. C* **2016**, *4*, 4346–4373.
- [18] F. Lucarini, M. Pastore, S. Vasylevskyi, M. Varisco, E. Solari, A. Crochet, K. M. Fromm, F. Zobi, A. Ruggi, *Chem. - A Eur. J.* **2017**, *23*, 6768–6771.
- [19] Y. Han, H. Fang, H. Jing, H. Sun, H. Lei, W. Lai, R. Cao, *Angew. Chemie - Int. Ed.* **2016**, *55*, 5457–5462.
- [20] E. A. Gibson, *Chem. Soc. Rev.* **2017**, *46*, 6194–6209.
- [21] N. Kaeffer, J. Massin, C. Lebrun, O. Renault, M. Chavarot-Kerlidou, V. Artero, *J. Am. Chem. Soc.* **2016**, *138*, 12308–12311.
- [22] V. Nikolaou, A. Charisiadis, G. Charalambidis, A. G. Coutsolelos, F. Odobel,

- J. Mater. Chem. A* **2017**, *5*, 21077–21113.
- [23] L. D’Amario, J. Föhlinger, G. Boschloo, L. Hammarström, *Chem. Sci.* **2017**, *9*, 223–230.
- [24] S. Piccinin, D. Rocca, M. Pastore, *J. Phys. Chem. C* **2017**, *121*, 22286–22294.
- [25] M. V. Sheridan, B. D. Sherman, R. L. Coppo, D. Wang, S. L. Marquard, K.-R. Wee, N. Y. Murakami Iha, T. J. Meyer, *ACS Energy Lett.* **2016**, *1*, 231–236.
- [26] J. T. Kirner, R. G. Finke, *J. Mater. Chem. A* **2017**, *5*, 19560–19592.
- [27] M. Pastore, F. De Angelis, *J. Am. Chem. Soc.* **2015**, *137*, 5798–5809.
- [28] F. Ronconi, Z. Syrgiannis, A. Bonasera, M. Prato, R. Argazzi, S. Caramori, V. Cristino, C. A. Bignozzi, *J. Am. Chem. Soc.* **2015**, *137*, 4630–4633.
- [29] Y. Gao, X. Ding, J. Liu, L. Wang, Z. Lu, L. Li, L. Sun, *J. Am. Chem. Soc.* **2013**, *135*, 4219–4222.
- [30] B. D. Sherman, Y. Xie, M. V. Sheridan, D. Wang, D. W. Shaffer, T. J. Meyer, J. J. Concepcion, *ACS Energy Lett.* **2017**, *2*, 124–128.
- [31] B. D. Sherman, M. V. Sheridan, K. R. Wee, S. L. Marquard, D. Wang, L.

- Alibabaei, D. L. Ashford, T. J. Meyer, *J. Am. Chem. Soc.* **2016**, *138*, 16745–16753.
- [32] L. Zhang, Y. Gao, X. Ding, Z. Yu, L. Sun, *ChemSusChem* **2014**, *7*, 2801–2804.
- [33] M. K. Nazeeruddin, A. Kay, I. Rodicio, R. Humphry-Baker, E. Müller, P. Liska, N. Vlachopoulos, M. Grätzel, *J. Am. Chem. Soc.* **1993**, *115*, 6382–6390.
- [34] A. Mishra, M. K. R. Fischer, P. Büuerle, *Angew. Chemie - Int. Ed.* **2009**, *48*, 2474–2499.
- [35] M. Pastore, E. Mosconi, S. Fantacci, F. De Angelis, *Curr. Org. Synth.* **2012**, *9*, 215–232.
- [36] K. Kakiage, Y. Aoyama, T. Yano, K. Oya, T. Kyomen, M. Hanaya, *Chem. Commun.* **2015**, *51*, 6315–6317.
- [37] S. Mathew, A. Yella, P. Gao, R. Humphry-Baker, B. F. E. Curchod, N. Ashari-Astani, I. Tavernelli, U. Rothlisberger, M. K. Nazeeruddin, M. Grätzel, *Nat. Chem.* **2014**, *6*, 242–247.
- [38] Z. Yao, M. Zhang, H. Wu, L. Yang, R. Li, P. Wang, *J. Am. Chem. Soc.* **2015**, *137*, 3799–3802.

- [39] K. S. V. Gupta, J. Zhang, G. Marotta, M. A. Reddy, S. P. Singh, A. Islam, L. Han, F. De Angelis, M. Chandrasekharam, M. Pastore, *Dye. Pigment.* **2015**, *113*, 536–545.
- [40] B. G. Kim, K. Chung, J. Kim, *Chem. - A Eur. J.* **2013**, *19*, 5220–5230.
- [41] B. Cecconi, N. Manfredi, T. Montini, P. Fornasiero, A. Abbotto, *European J. Org. Chem.* **2016**, *2016*, 5194–5215.
- [42] G. F. Moore, J. D. Blakemore, R. L. Milot, J. F. Hull, H. E. Song, L. Cai, C. A. Schmuttenmaer, R. H. Crabtree, G. W. Brudvig, *Energy Environ. Sci.* **2011**, *4*, 2389–2392.
- [43] J. R. Swierk, D. D. Méndez-Hernández, N. S. McCool, P. Liddell, Y. Terazono, I. Pahk, J. J. Tomlin, N. V Oster, T. A. Moore, A. L. Moore, et al., *Proc. Natl. Acad. Sci.* **2015**, *112*, 1681–1686.
- [44] B. J. Brennan, Y. C. Lam, P. M. Kim, X. Zhang, G. W. Brudvig, *ACS Appl. Mater. Interfaces* **2015**, *7*, 16124–16130.
- [45] D. Khusnutdinova, A. M. Beiler, B. L. Wadsworth, S. I. Jacob, G. F. Moore, *Chem. Sci.* **2016**, *8*, 253–259.
- [46] M. Yamamoto, Y. Nishizawa, P. Chábera, F. Li, T. Pascher, V. Sundström, L. Sun, H. Imahori, *Chem. Commun.* **2016**, *52*, 13702–13705.

- [47] S. H. Kang, M. J. Jeong, Y. K. Eom, I. T. Choi, S. M. Kwon, Y. Yoo, J. Kim, J. Kwon, J. H. Park, H. K. Kim, *Adv. Energy Mater.* **2017**, *7*, 1602117.
- [48] D. Jacquemin, E. A. Perpète, G. E. Scuseria, I. Ciofini, C. Adamo, *J. Chem. Theory Comput.* **2008**, *4*, 123–135.
- [49] S. Fantacci, F. De Angelis, *Coord. Chem. Rev.* **2011**, *255*, 2704–2726.
- [50] M. Pastore, S. Fantacci, F. De Angelis, **2010**, 22742–22750.
- [51] Y. Bai, I. Mora-Seró, F. De Angelis, J. Bisquert, P. Wang, *Chem. Rev.* **2014**, *114*, 10095–10130.
- [52] J. Calbo, M. Pastore, E. Mosconi, E. Ortí, F. De Angelis, *Phys. Chem. Chem. Phys.* **2014**, *16*, 4709–4719.
- [53] F. Labat, T. Le Bahers, I. Ciofini, C. Adamo, *Acc. Chem. Res.* **2012**, *45*, 1268–1277.
- [54] F. Ambrosio, N. Martsinovich, A. Troisi, *J. Phys. Chem. Lett.* **2012**, *3*, 1531–1535.
- [55] E. Ronca, G. Marotta, M. Pastore, F. De Angelis, *J. Phys. Chem. C* **2014**, *118*, 16927–16940.
- [56] W. R. Duncan, O. V. Prezhdo, *Annu. Rev. Phys. Chem.* **2007**, *58*, 143–184.

- [57] W. R. Duncan, C. F. Craig, O. V. Prezhdo, *J. Am. Chem. Soc.* **2007**, *129*, 8528–8543.
- [58] J. Jiang, J. A. Spies, J. R. Swierk, A. J. Matula, K. P. Regan, N. Romano, B. J. Brennan, R. H. Crabtree, V. S. Batista, C. A. Schmuttenmaer, et al., *J. Phys. Chem. C* **2018**, *122*, 13529–13539.
- [59] M. Pastore, T. Duchanois, L. Liu, A. Monari, X. Assfeld, S. Haacke, P. C. Gros, *Phys. Chem. Chem. Phys.* **2016**, *18*, 28069–28081.
- [60] L. G. C. Rego, V. S. Batista, *J. Am. Chem. Soc.* **2003**, *125*, 7989–7997.
- [61] M. Pastore, A. Selloni, S. Fantacci, F. De Angelis, *Top. Curr. Chem.* **2014**, *347*, 1–46.
- [62] T. Dos Santos, A. Morandeira, S. Koops, A. J. Mozer, G. Tsekouras, Y. Dong, P. Wagner, G. Wallace, J. C. Earles, K. C. Gordon, et al., *J. Phys. Chem. C* **2010**, *114*, 3276–3279.
- [63] R. L. Milot, G. F. Moore, R. H. Crabtree, G. W. Brudvig, C. A. Schmuttenmaer, *J. Phys. Chem. C* **2013**, *117*, 21662–21670.
- [64] M. J. Frisch, G. W. Trucks, H. B. Schlegel, G. E. Scuseria, M. A. Robb, J. R. Cheeseman, G. Scalmani, V. Barone, B. Mennucci, G. A. Petersson, et al., *Gaussian 09, Revis. D.01*, Gaussian, Inc., Wallingford CT, 2013. **n.d.**

- [65] V. Barone, M. Cossi, *J. Phys. Chem. A* **1998**, *102*, 1995–2001.
- [66] M. Pastore, E. Mosconi, F. De Angelis, M. Grätzel, *J. Phys. Chem. C* **2010**, *114*, 7205–7212.
- [67] A. D. Becke, *J. Chem. Phys.* **1993**, *98*, 5648–5652.
- [68] C. Adamo, V. Barone, *J. Chem. Phys.* **1999**, *110*, 6158–6170.
- [69] A. V. Krukau, O. A. Vydrov, A. F. Izmaylov, G. E. Scuseria, *J. Chem. Phys.* **2006**, *125*, 224106.
- [70] J. Heyd, G. E. Scuseria, *J. Chem. Phys.* **2004**, *121*, 1187–1192.
- [71] A. D. Boese, J. M. L. Martin, *J. Chem. Phys.* **2004**, *121*, 3405–3416.
- [72] J. Tao, J. P. Perdew, V. N. Staroverov, G. E. Scuseria, *Phys. Rev. Lett.* **2003**, *91*, 146401.
- [73] Y. Zhao, D. G. Truhlar, *Theor. Chem. Acc.* **2008**, *120*, 215–241.
- [74] B. J. Lynch, P. L. Fast, M. Harris, D. G. Truhlar, **2000**, *104*, 0–4.
- [75] T. Yanai, D. P. Tew, N. C. Handy, *Chem. Phys. Lett.* **2004**, *393*, 51–57.
- [76] J. Da Chai, M. Head-Gordon, *Phys. Chem. Chem. Phys.* **2008**, *10*, 6615–6620.

- [77] S. Grimme, *J. Comput. Chem.* **2006**, *27*, 1787–1799.
- [78] O. A. Vydrov, G. E. Scuseria, *J. Chem. Phys.* **2006**, *125*, 234109.
- [79] M. Pastore, F. De Angelis, *Top. Curr. Chem.* **2014**, *352*, 151–236.
- [80] S. Tortorella, M. M. Talamo, A. Cardone, M. Pastore, F. De Angelis, *J. Phys. Condens. Matter* **2016**, *28*, 074005.
- [81] A. Vittadini, A. Selloni, F. P. Rotzinger, M. Grätzel, *Phys. Rev. Lett.* **1998**, *81*, 2954–2957.
- [82] G. te Velde, F. M. Bickelhaupt, E. J. Baerends, C. Fonseca Guerra, S. J. A. van Gisbergen, J. G. Snijders, T. Ziegler, *J. Comput. Chem.* **2001**, *22*, 931–967.
- [83] C. Fonseca Guerra, J. G. Snijders, G. Te Velde, E. J. Baerends, *Theor. Chem. Acc.* **1998**, *99*, 391–403.
- [84] J. P. Perdew, K. Burke, M. Ernzerhof, *Phys. Rev. Lett.* **1996**, *77*, 3865–3868.
- [85] S. Grimme, S. Ehrlich, L. Goerigk, *J. Comput. Chem.* **2011**, *32*, 1456–1465.
- [86] L. Lasser, E. Ronca, M. Pastore, F. De Angelis, J. Cornil, R. Lazzaroni, D. Beljonne, *J. Phys. Chem. C* **2015**, *119*, 9899–9909.
- [87] G. Marotta, M. A. Reddy, S. P. Singh, A. Islam, L. Han, F. De Angelis, M.

- Pastore, M. Chandrasekharam, *ACS Appl. Mater. Interfaces* **2013**, *5*, 9635–9647.
- [88] J. P. Muscat, D. M. Newns, *Prog. Surf. Sci.* **1978**, *9*, 1–43.
- [89] C. Rimington, S. F. Mason, O. Kennard, *Spectrochim. Acta* **2002**, *12*, 65–77.
- [90] M. Gouterman, *J. Chem. Phys.* **1959**, *30*, 1139–1161.
- [91] M. Gouterman, *J. Mol. Spectrosc.* **1961**, *6*, 138–163.
- [92] E. R. Davidson, A. A. Jarzęcki, *Chem. Phys. Lett.* **1998**, *285*, 155–159.
- [93] C. Angeli, M. Pastore, *J. Chem. Phys.* **2011**, *134*, 184302.
- [94] A. A. El-Azhary, H. U. Suter, *J. Phys. Chem.* **1996**, *3654*, 15056–15063.
- [95] P. Olszowski, L. Zając, S. Godlewski, B. Such, R. Jöhr, T. Glatzel, E. Meyer, M. Szymonski, *J. Phys. Chem. C* **2015**, *119*, 21561–21566.
- [96] M. Pastore, S. Fantacci, F. De Angelis, *J. Phys. Chem. C* **2013**, *117*, 3685–3700.
- [97] D. Escudero, I. Duchemin, X. Blase, D. Jacquemin, *J. Phys. Chem. Lett.* **2017**, *8*, 936–940.
- [98] P. Umari, L. Giacomazzi, F. De Angelis, M. Pastore, S. Baroni, *J. Chem. Phys.* **2013**, *139*, 014709.

[99] M. Marsili, E. Mosconi, F. De Angelis, P. Umari, **2016**, DOI  
10.1103/PhysRevB.95.075415.